Multifractal Formalism based on the Continuous Wavelet Transform

Alain Arneodo[1,2,3], Benjamin Audit[1,2,3], Pierre Kestener[4] and Stéphane Roux[1,3].

[1]Université de Lyon, F-69000, Lyon, France; [2]Laboratoire Joliot-Curie and [3]Laboratoire de Physique, CNRS, ENS-Lyon, 46 Allée d'Italie, F-69007 Lyon, France; [4]DAPNIA, CEA, Centre d'Etudes Nucléaire de Saclay, Gif-sur-Yvette, France.

Abstract

The multifractal formalism was introduced in the context of fully-developed turbulence data analysis and modeling to account for the experimental observation of some deviation to Kolmogorov theory (K41) of homogenous and isotropic turbulence (Frisch, 1995). The predictions of various multiplicative cascade models, including the weighted curdling (binomial) model proposed by Mandelbrot (1974), were tested using box-counting (BC) estimates of the so-called $f(\alpha)$ singularity spectrum of the dissipation field (Meneveau & Sreenivasan, 1991). Alternatively, the intermittent nature of the velocity fluctuations were investigated via the computation of the $D(h)$ singularity spectrum using the structure function (SF) method (Parisi & Frisch, 1985). Unfortunately, both types of studies suffered from severe insufficiencies. On the one hand, they were mostly limited by one point probe measurements to the analysis of one (longitudinal) velocity component and to some 1D surrogate approximation of the dissipation (Aurell et al., 1992). On the other hand, both the BC and SF methodologies have intrinsic limitations and fail to fully characterize the corresponding singularity spectrum since only the strongest singularities are a priori amenable to these techniques (Arneodo et al., 1995b; Bacry et al., 1993; Muzy et al., 1993, 1994). In the early nineties, a statistical approach based on the continuous wavelet transform was proposed as a unified multifractal description of singular measures and multi-affine functions (Arneodo et al., 1995b; Bacry et al., 1993; Muzy et al., 1993, 1994). Applications of the so-called *wavelet transform modulus maxima* (WTMM) method have already provided insight into a wide variety of problems, e.g., fully developed turbulence, econophysics, meteorology, physiology and DNA sequences (Arneodo et al., 2002). Let us note that alternative approaches to the multifractal description have been developed using discrete wavelet bases (Abry et al., 2000, 2002a,b; Veitch & Abry, 1999) including the recent use of wavelet leaders (Jaffard et al., 2006; Wendt & Abry, 2007; Wendt et al., 2007). Later on, the WTMM method was generalized to 2D for multifractal analysis of rough surfaces (Arneodo et al., 2000; Decoster et al., 2000), with very promising results in the context of the geophysical study of the intermittent nature of satellite images of the cloud structure (Arneodo et al., 1999a, 2003; Roux et al., 2000) and the medical assist in the diagnosis in digitized mammograms (Arneodo et al., 2003; Kestener et al., 2001). Recently, the WTMM method has been further extended to 3D scalar as well as 3D vector field analysis and applied to 3D numerical data issue from isotropic turbulence direct numerical simulations (DNS) (Kestener & Arneodo, 2003, 2004, 2007).

Contents

1 The Continuous Wavelet Transform

1.1 Introduction

The continuous wavelet transform (WT) is a mathematical technique introduced in signal analysis in the early 1980s (Goupillaud et al., 1984; Grossmann & Morlet, 1984). Since then, it has been the subject of considerable theoretical developments and practical applications in a wide variety of fields. The WT has been early recognized as a mathematical microscope that is well adapted to reveal the hierarchy that governs the spatial distribution of singularities of multifractal measures (Arneodo et al., 1988, 1989, 1992). What makes the WT of fundamental use in the present study is that its singularity scanning ability equally applies to singular functions than to singular measures (Arneodo et al., 1988, 1989, 1992; Holschneider, 1988; Holschneider & Tchamitchian, 1990; Jaffard, 1989, 1991; Mallat & Hwang, 1992; Mallat & Zhong, 1992). This has led Alain Arneodo and his collaborators (Arneodo et al., 1995b; Bacry et al., 1993; Muzy et al., 1991, 1993, 1994) to elaborate a unified thermodynamic description of multifractal distributions including measures and functions, the so-called Wavelet Transform Modulus Maxima (WTMM) method. By using wavelets instead of boxes, one can take advantage of the freedom in the choice of these "generalized oscillating boxes" to get rid of possible (smooth) polynomial behavior that might either mask singularities or perturb the estimation of their strength h (Hölder exponent), remedying in this way for one of the main failures of the classical multifractal methods (*e.g.* the box-counting algorithms in the case of measures and the structure function method in the case of functions (Arneodo et al., 1995b; Bacry et al., 1993; Muzy et al., 1993, 1994)). The other fundamental advantage of using wavelets is that the skeleton defined by the WTMM (Mallat & Hwang, 1992; Mallat & Zhong, 1992), provides an adaptative space-scale partitioning from which one can extract the $D(h)$ singularity spectrum via the Legendre transform of the scaling exponents $\tau(q)$ (q real, positive as well as negative) of some partition functions defined from the WT skeleton. We refer the reader to Bacry et al. (1993), Jaffard (1997a,b) for rigorous mathematical results and to Hentschel (1994) for the theoretical treatment of random multifractal functions.

1.2 Definition

The WT is a space-scale analysis which consists in expanding signals in terms of *wavelets* which are constructed from a single function, the *analyzing wavelet* ψ, by means of translations and dilations. The WT of a real-valued function f is defined as (Goupillaud et al., 1984; Grossmann & Morlet, 1984):

$$T_\psi[f](x_0,a) = \frac{1}{a}\int_{-\infty}^{+\infty} f(x)\psi(\frac{x-x_0}{a})dx \ , \tag{1}$$

where x_0 is the space parameter and a (>0) the scale parameter. The analyzing wavelet ψ is generally chosen to be well localized in both space and frequency. Usually ψ is required to be of zero mean for the WT to be invertible. But for the particular purpose of singularity tracking that is of interest here, we will further require ψ to be orthogonal to low-order polynomials (Arneodo et al., 1995b; Bacry et al., 1993; Holschneider & Tchamitchian, 1990; Jaffard, 1989, 1991; Mallat & Hwang, 1992; Mallat & Zhong, 1992; Muzy et al., 1991, 1993, 1994):

$$\int_{-\infty}^{+\infty} x^m\psi(x)dx = 0 \ , \quad 0 \le m < n_\psi \ . \tag{2}$$

As originally pointed out by Mallat and collaborators (Mallat & Hwang, 1992; Mallat & Zhong, 1992), for the specific purpose of analyzing the regularity of a function, one can get rid of the redundancy of the WT by concentrating on the WT skeleton defined by its modulus maxima only. These maxima are defined, at each scale a, as the local maxima of $|T_\psi[f](x,a)|$ considered as a function of x. As illustrated in Fig. 2(e,f), these WTMM are disposed on connected curves in the space-scale (or time-scale) half-plane, called *maxima lines*. Let us define $\mathcal{L}(a_0)$ as the set of all the maxima lines that exist at the scale a_0 and which contain maxima at any scale $a \le a_0$. An

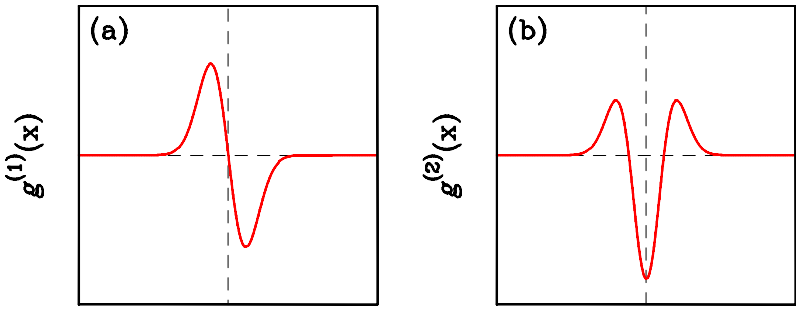

Figure 1 Set of analyzing wavelets $\psi(x)$ that can be used in Eq. (1). (a) $g^{(1)}$ and (b) $g^{(2)}$ as defined in Eq. (3).

important feature of these maxima lines, when analyzing singular functions, is that there is at least one maxima line pointing towards each singularity (Mallat & Hwang, 1992; Mallat & Zhong, 1992; Muzy et al., 1994).

1.3 Analyzing Wavelets

There are almost as many analyzing wavelets as applications of the continuous WT (Arneodo et al., 1988, 1989, 1992, 1995b; Bacry et al., 1993; Muzy et al., 1991, 1993, 1994). A commonly used class of analyzing wavelets is defined by the successive derivatives of the Gaussian function:

$$g^{(N)}(x) = \frac{d^N}{dx^N} e^{-x^2/2} \ , \tag{3}$$

for which $n_\psi = N$ and more specifically $g^{(1)}$ and $g^{(2)}$ that are illustrated in Fig. 1(a,b). Note that the WT of a signal f with $g^{(N)}$ (Eq. (3)) takes the following simple expression:

$$\begin{aligned} T_{g^{(N)}}[f](x,a) &= \frac{1}{a}\int_{-\infty}^{+\infty} f(y) g^{(N)}\left(\frac{y-x}{a}\right) dy, \\ &= a^N \frac{d^N}{dx^N} T_{g^{(0)}}[f](x,a). \end{aligned} \tag{4}$$

Equation (4) shows that the WT computed with $g^{(N)}$ at scale a is nothing but the Nth derivative of the signal $f(x)$ smoothed by a dilated version $g^{(0)}(x/a)$ of the Gaussian function. This property is at the heart of various applications of the WT microscope as a very efficient multi-scale singularity tracking technique (Arneodo et al., 2002).

1.4 Scanning Singularities with the Wavelet Transform Modulus Maxima

The strength of the singularity of a function f at point x_0 is given by the *Hölder* exponent, *i.e.*, the largest exponent such that there exists a polynomial $P_n(x-x_0)$ of order $n < h(x_0)$ and a constant $C > 0$, so that for any point x in a neighborhood of x_0, one has (Bacry et al., 1993; Holschneider & Tchamitchian, 1990; Jaffard, 1989, 1991; Mallat & Hwang, 1992; Mallat & Zhong, 1992; Muzy et al., 1994):

$$|f(x) - P_n(x-x_0)| \leq C|x-x_0|^h \ . \tag{5}$$

If f is n times continuously differentiable at the point x_0, then one can use for the polynomial $P_n(x-x_0)$, the order-n Taylor series of f at x_0 and thus prove that $h(x_0) > n$. Thus $h(x_0)$ measures how irregular the function f is at the point x_0. The higher the exponent $h(x_0)$, the more regular the function f.

The main interest in using the WT for analyzing the regularity of a function lies in its ability to be blind to polynomial behavior by an appropriate choice of the analyzing wavelet ψ. Indeed, let us assume that according to Eq. (5), f has, at the point x_0, a local scaling (Hölder) exponent $h(x_0)$; then, assuming that the singularity is not oscillating (Arneodo et al., 1997a, 1998b; Mallat & Zhong, 1992), one can easily prove that the local behavior of f is mirrored by the WT which locally behaves like (Arneodo et al., 1995b; Bacry et al., 1993; Holschneider & Tchamitchian, 1990; Jaffard, 1989, 1991, 1997a,b; Mallat & Hwang, 1992; Mallat & Zhong, 1992; Muzy et al., 1991, 1993, 1994) :

$$T_\psi[f](x_0, a) \sim a^{h(x_0)} \, , a \to 0^+ \, , \tag{6}$$

provided $n_\psi > h(x_0)$, where n_ψ is the number of vanishing moments of ψ (Eq. (2)). Therefore one can extract the exponent $h(x_0)$ as the slope of a log-log plot of the WT amplitude versus the scale a. On the contrary, if one chooses $n_\psi < h(x_0)$, the WT still behaves as a power-law but with a scaling exponent which is n_ψ :

$$T_\psi[f](x_0, a) \sim a^{n_\psi} \, , a \to 0^+ \, . \tag{7}$$

Thus, around a given point x_0, the faster the WT decreases when the scale goes to zero, the more regular f is around that point. In particular, if $f \in C^\infty$ at x_0 ($h(x_0) = +\infty$), then the WT scaling exponent is given by n_ψ, *i.e.* a value which is dependent on the shape of the analyzing wavelet. According to this observation, one can hope to detect the points where f is smooth by just checking the scaling behavior of the WT when increasing the order n_ψ of the analyzing wavelet (Arneodo et al., 1995b; Bacry et al., 1993; Muzy et al., 1991, 1993, 1994).

Remark

A very important point (at least for practical purpose) raised by Mallat and Hwang (Mallat & Hwang, 1992) is that the local scaling exponent $h(x_0)$ can be equally estimated by looking at the value of the WT modulus along a maxima line converging towards the point x_0. Indeed one can prove that both Eqs. (6) and (7) still hold when following a maxima line from large down to small scales (Mallat & Hwang, 1992; Mallat & Zhong, 1992).

2 The Wavelet Transform Modulus Maxima Method for Multifractal Analysis

2.1 Singularity Spectrum

As originally defined by Parisi & Frisch (1985), the multifractal formalism of multi-affine functions amounts to compute the so-called *singularity spectrum* $D(h)$ defined as the Hausdorff dimension of the set where the Hölder exponent is equal to h (Arneodo et al., 1995b; Bacry et al., 1993; Muzy et al., 1994):

$$D(h) = dim_H\{x \, , \, h(x) = h\} \, , \tag{8}$$

where h can take, *a priori*, positive as well as negative real values (*e.g.*, the Dirac distribution $\delta(x)$ corresponds to the Hölder exponent $h(0) = -1$) (Jaffard, 1997a).

2.2 The WTMM Method

A natural way of performing a multifractal analysis of fractal functions consists in generalizing the "classical" multifractal formalism (Collet et al., 1987; Grassberger et al., 1988; Halsey et al., 1986; Paladin & Vulpiani, 1987; Rand, 1989) using wavelets instead of boxes. By taking advantage of the freedom in the choice of the "generalized oscillating boxes" that are the wavelets, one can hope to get rid of possible smooth behavior that could mask singularities or perturb the estimation of their strength h. But the major difficulty with respect to box-counting techniques (Argoul et al., 1990; Farmer et al., 1983; Grassberger & Procaccia, 1983; Grassberger et al., 1988; Meneveau & Sreenivasan, 1991) for singular measures, consists in defining a covering of the support of

the singular part of the function with our set of wavelets of different sizes. As emphasized in Refs. (Arneodo et al., 1995b; Bacry et al., 1993; Muzy et al., 1991, 1993, 1994), the branching structure of the WT skeletons of fractal functions in the (x, a) half-plane enlightens the hierarchical organization of their singularities (Figs. 2(e,f)). The WT skeleton can thus be used as a guide to position, at a considered scale a, the oscillating boxes in order to obtain a partition of the singularities of f. The wavelet transform modulus maxima (WTMM) method amounts to compute the following partition function in terms of WTMM coefficients (Arneodo et al., 1995b; Bacry et al., 1993; Muzy et al., 1991, 1993, 1994):

$$Z(q,a) = \sum_{l \in \mathcal{L}(a)} \left(\sup_{\substack{(x,a') \in l \\ a' \leq a}} |T_\psi[f](x,a')| \right)^q , \tag{9}$$

where $q \in \mathbb{R}$ and the sup can be regarded as a way to define a scale adaptative "Hausdorff-like" partition. Now from the deep analogy that links the multifractal formalism to thermodynamics (Arneodo et al., 1995b; Bohr & Tèl, 1988), one can define the exponent $\tau(q)$ from the power-law behavior of the partition function:

$$Z(q,a) \sim a^{\tau(q)} , \quad a \to 0^+ , \tag{10}$$

where q and $\tau(q)$ play respectively the role of the inverse temperature and the free energy. The main result of this wavelet-based multifractal formalism is that in place of the energy and the entropy (*i.e.* the variables conjugated to q and τ), one has h, the Hölder exponent, and $D(h)$, the singularity spectrum. This means that the singularity spectrum of f can be determined from the Legendre transform of the partition function scaling exponent $\tau(q)$ (Bacry et al., 1993; Jaffard, 1997a,b):

$$D(h) = \min_q (qh - \tau(q)) . \tag{11}$$

2.3 Monofractal versus Multifractal Functions

From the properties of the Legendre transform, it is easy to see that *homogeneous* monofractal functions that involve singularities of unique Hölder exponent $h = \partial\tau/\partial q$, are characterized by a $\tau(q)$ spectrum which is a *linear* function of q (Fig. 3(c)). On the contrary, a *nonlinear* $\tau(q)$ curve is the signature of nonhomogeneous functions that exhibit *multifractal* properties, in the sense that the Hölder exponent $h(x)$ is a fluctuating quantity that depends upon the spatial position x (Fig. 3(c)). As illustrated in Fig. 3(d), the $D(h)$ singularity spectrum of a multifractal function displays a single humped shape that characterizes intermittent fluctuations corresponding to Hölder exponent values spanning a whole interval $[h_{min}, h_{max}]$, where h_{min} and h_{max} are the Hölder exponents of the strongest and weakest singularities respectively.

2.4 Applications of the WTMM Method

2.4.1 DNA sequences: Monofractality of DNA walks

A DNA sequence is a four-letter (A, C, G ,T) text where A, C, G and T stand for the bases adenine, cytosine, guanine and thymine respectively. A popular method to graphically portray the genetic information stored in DNA sequences is to used the so-called "DNA walk" representation (Peng et al., 1992). It consists first in converting the DNA text into a binary sequence by coding for example with $\chi(i) = 1$ at a given nucleotide positions and $\chi(i) = -1/3$ at other positions (Voss, 1992), and then in defining the graph of the DNA walk by the cumulative variables $f(n) = \sum_{i=1}^{n} \chi(i)$. The DNA walk obtained with the "G" mononucleotide coding for the largest intron of the human dystrophin gene is shown in Fig. 2(a) for illustration. Fig. 2(c) illustrates the WT when using an analyzing wavelet of sufficiently high order, namely $g^{(2)}$ ($n_\psi = 2$), to get rid of the linear trends in the DNA walk landscape inherent to the heterogeneity of composition of genomic

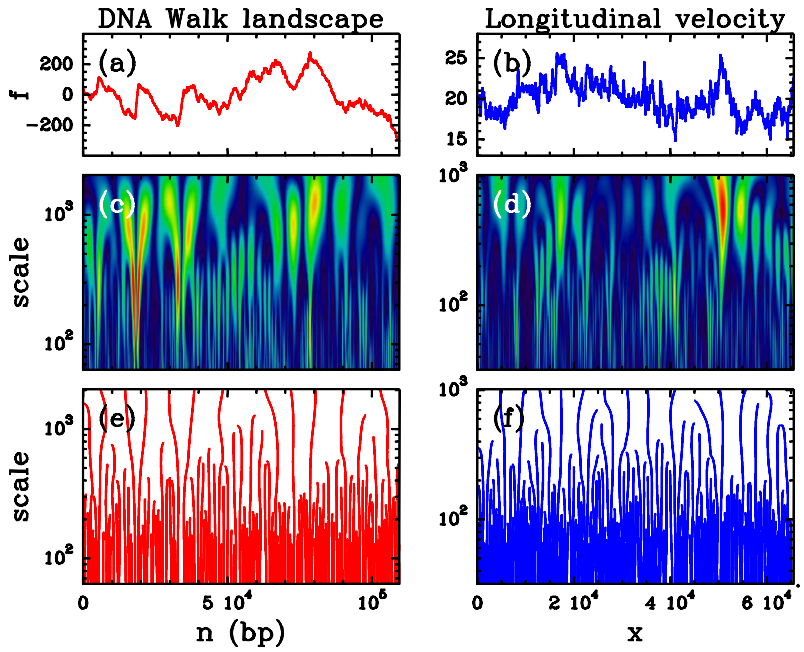

Figure 2 WT of monofractal and multifractal functions.
DNA walk: (a) DNA walk $f(x)$ of the largest intron of human dystrophin gene ($L = 109574$) using the "G" mononucleotide coding; (c) WT of DNA walk landscape color coded, independently at each scale a, using 256 colors from black ($|T_\psi| = 0$) to red ($\max |T_\psi|$); (e) WT skeleton defined by the set of all maxima lines.
Fully developed turbulence: (b) Longitudinal velocity signal recorded in the Modane wind-tunnel experiment ($R_\lambda \simeq 2000$) over about two integral scales; (d) WT of the velocity signal in (b) using the same color coding as in (c); (f) corresponding WT skeleton.
The analyzing wavelet is the Mexican hat $g^{(2)}$ (Eq. (3)).

sequences (Arneodo et al., 1995a, 1996). Fig. 3(a) displays some plots of $\log_2 Z(q,a)$ vs $\log_2(a)$ for different values of q, where the partition function $Z(q,a)$ has been computed on the WTMM skeleton (Fig. 2(e)), according to the definition (Eq. (9)) for a set of 2184 human introns of size $L \geq 800$bp. Using a linear regression fit, we then obtain the slopes $\tau(q)$ of these graphs. As shown in Fig. 3(c), when plotted versus q, the data for the exponents $\tau(q)$ consistently fall on a straight line that is remarkably fitted by

$$\tau(q) = qH - 1 \,, \tag{12}$$

with $H = 0.60 \pm 0.02$. From the Legendre transform of this linear $\tau(q)$ (Eq. (11)), one gets a $D(h)$ singularity spectrum that reduces to a single point:

$$\begin{aligned} D(h) &= 1 \quad \text{if} \quad h = H \,, \\ &= -\infty \quad \text{if} \quad h \neq H \,, \end{aligned} \tag{13}$$

as the signature of a nowhere differentiable homogeneous fractal signal with a unique Hölder exponent $h = H = 0.60$. Note that similar good estimates are obtained when using analyzing wavelets of different order (*e.g.* $g^{(3)}$).

Within the perspective of confirming the monofractality of DNA walks, we have studied the probability density function (pdf) of wavelet coefficient values $\rho_a(T_{g^{(2)}}(.,a))$, as computed at a fixed scale a in the fractal scaling range. According to the monofractal scaling properties, one expects these pdfs to satisfy the self-similarity relationship (Arneodo et al., 1995a, 1996, 2002):

$$a^H \rho_a(a^H T) = \rho(T) \,, \tag{14}$$

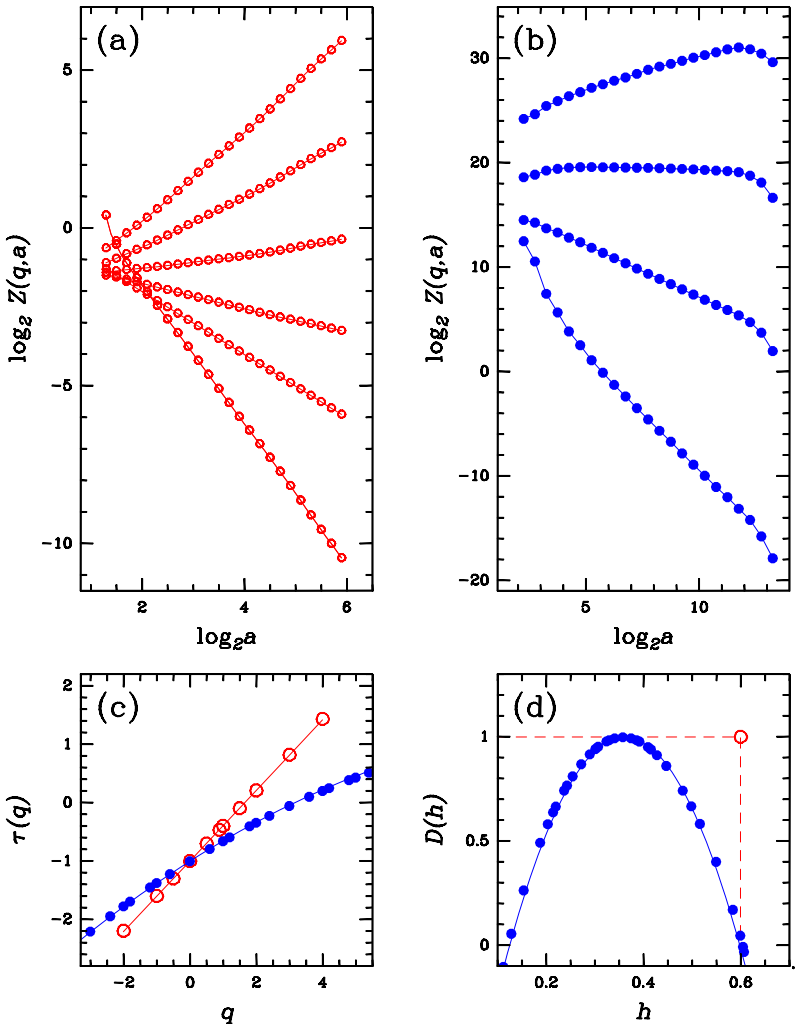

Figure 3 Determination of the $\tau(q)$ and $D(h)$ multifractal spectra of the "G" DNA walks of a set of 2184 human introns ($L \geq 800$bp) ($\circ$) and of the turbulent velocity signals ($\bullet$) using the WTMM method. $\log_2 Z(q,a)$ vs $\log_2 a$ for, from bottom to top, $q = -2$, -1, 0, 1, 2, 3 and 4 in (a) and for $q = -3$, 0, 3 and 6 in (b). (c) $\tau(q)$ vs q; the solid lines correspond respectively to a monofractal spectrum $\tau(q) = qH - 1$ with $H = 0.60 \pm 0.02$ (red) and to a quadratic multifractal spectrum $\tau(q) = c_1 q - \frac{c_2}{2} q^2 - 1$ with $c_1 = 0.36 \pm 0.02$ and a non zero value for the intermittent coefficient $c_2 = 0.028 \pm 0.003$ (blue). (d) $D(h)$ vs h; while the singularity spectrum of the monofractal DNA walk landscape reduces to a point ($D(h = 0.6) = 1$ and 0 elsewhere, $\circ$), it has a parabolic shape and extends from $h_{min} = 0.12$ to $h_{max} = 0.60$ as the signature of the "intermittent" multifractal nature of Eulerian turbulence ($\bullet$). The analyzing wavelet is $g^{(2)}$ (Eq. (3)).

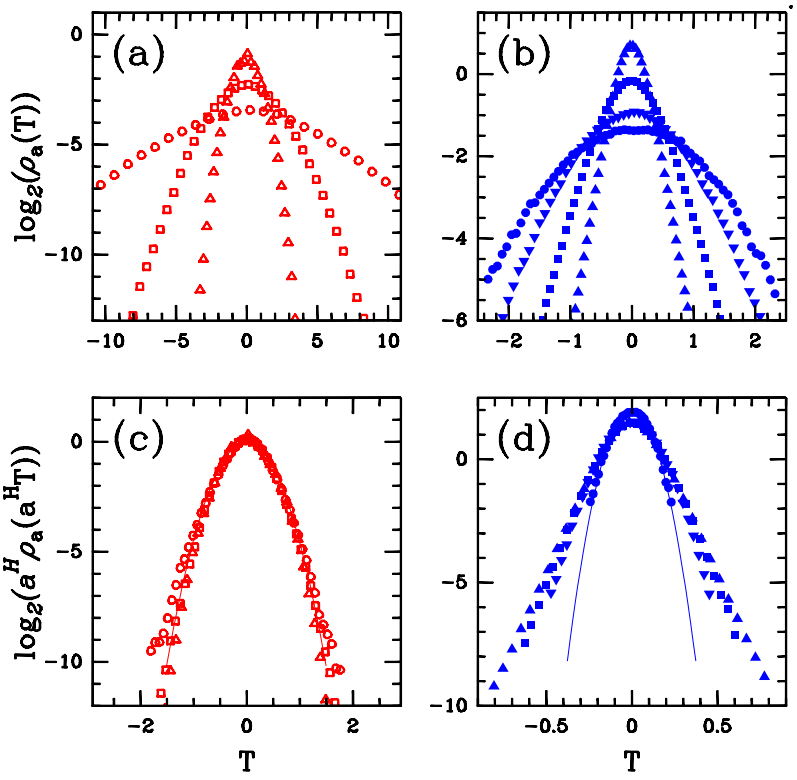

Figure 4 Probability density functions of the wavelet coefficient values of the "G" DNA walk of 2834 human introns ($L \geq 600$) (red open symbols) and of the turbulent velocity signal (blue filled symbols). (a) and (b) $\rho_a(T)$ for the sets of scales $a = 4$ (△), 16 (□), 64 (○) and $a = 27$ (▲), 144 (■), 760 (▼), 3993 (●). (c) and (d) $a^H \rho_a(a^H T)$ for the same sets of scales; $H = 0.60$ in (c) and $H = 1/3$ in (d). The analyzing wavelet is $g^{(2)}$.

where $\rho(T)$ is a "universal" pdf (actually the pdf obtained at scale $a = 1$) that does not depend on the scale parameter a. As shown in Fig. 4(a,c), when plotting $a^H \rho_a(a^H T)$ vs T, all the ρ_a curves corresponding to different scales (Fig. 4(a)) remarkably collapse on a unique curve when using a unique exponent $H = 0.60$ (Fig. 4(c)). Furthermore the so-obtained universal curve cannot be distinguished from a parabola in semi-log representation as the signature of monofractal Gaussian statistics. Therefore, the fluctuations of DNA walks about the composition induced linear trends cannot be distinguished from persistent fractional Brownian motion (fBm) $B_{H=0.60}$ that display long-range correlations (LRC) ($H > 0.5$) (Arneodo et al., 1996, 2002; Muzy et al., 1994). Similar LRC were found in non-coding sequences as well as in coding regions (*e.g.* coding exons) in eukaryotic genomes (but not for eubacterial sequences for which $H = 0.5$) as the signature of nucleosomal structure, the first step of compaction of DNA in eukaryotic nuclei (Audit et al., 2001, 2002).

2.4.2 Fully developed turbulence

It is now well accepted (Frisch, 1995) that in the fully developed regime, a turbulent flow is likely to be in a universal state that can be experimentally characterized by statistical quantities such as the multifractal spectra $\tau(q)$ and $D(h)$. For more than thirty years, one of the main features recognized experimentally is the intermittency of small scales (Frisch, 1995; Meneveau & Sreenivasan, 1991; Monin & Yaglom, 1975) which manifests in a significant departure of the experimental velocity data from the monofractal prediction $\tau(q) = q/3 - 1$ of Kolmogorov (K41) (Kolmogorov, 1941) based on the homogeneity assumption that, at each point of the fluid, the longitudinal velocity

increments have the same scaling behavior $\delta v_l(x) \sim l^{1/3}$, which yields the well known $E(k) \sim k^{-5/3}$ energy spectrum (Frisch, 1995). The pioneering studies (Anselmet et al., 1984; Frisch, 1995) were performed using the structure functions method which, as discussed in Muzy et al. (1993), intrinsically fails to fully characterize the $D(h)$ singularity spectrum.

In Figs. 2(b,d,f), 3(b,c,d) and 4(b,d) are reported the results of a multifractal analysis of single point longitudinal velocity data from high Reynolds 3D turbulence using the WTMM method (Arneodo et al., 1998a,c, 1999b; Delour et al., 2001). The data were obtained by Gagne and collaborators in the large wind tunnel S1 of ONERA at Modane. The Taylor scale based Reynolds number is $R_\lambda \simeq 2000$ and the extent of the inertial range following approximately the Kolmogorov $k^{-5/3}$ law is about four decades (integral scale $L \simeq 7$m, dissipation scale $\eta \simeq 0.27$mm). In Fig. 2(b) is illustrated a sample of the longitudinal velocity signal of length of about two integral scales, when using the Taylor hypothesis (Frisch, 1995). The corresponding WT and WT skeleton as computed with $g^{(2)}$ are shown in Figs. 2(d) and 2(f) respectively. As shown in Fig. 3(b), when plotted versus the scale parameter a in a logarithmic representation, the annealed average over 28000 integral scales of the partition functions $Z(q,a)$ displays a well defined scaling behavior in the inertial range for a rather wide range of q values: $-4 \leq q \leq 7$. When processing to a linear regression fit of the data, one gets a non-linear $\tau(q)$ spectrum, the hallmark of multifractal scaling, that is well approximated by the quadratic spectrum of log-normal processes:

$$\tau(q) = c_1 q - \frac{c_2}{2} q^2 - d \; , \tag{15}$$

with $c_1 = 0.36 \pm 0.02$, $c_2 = 0.028 \pm 0.003$ and where $d = 1$ is the spatial dimension (1D cut of the 3D velocity field). Similar, quantitative agreement is observed for the $D(h)$ singularity spectrum in Fig. 3(d) which displays a remarkable parabolic shape:

$$D(h) = d - \frac{(h + c_1)^2}{2c_2} \; , \tag{16}$$

that characterizes intermittent fluctuations corresponding to Hölder exponent values ranging from $h_{min} = 0.12$ to $h_{max} = 0.60$, the largest dimension $D(h(q = 0)) = -\tau(0) = 0.999 \pm 0.001 = d$ being attained for $h = c_1 = 0.36 \pm 0.02$, *i.e.*, a value which is slightly larger than the K41 prediction $h = 1/3$. This multifractal diagnosis is confirmed in Fig. 4(b) where the pdf of WT coefficients has a shape which evolves across scales from Gaussian at large scale to more intermittent profiles with stretched exponential-like tails at smaller scales. As illustrated in Fig. 4(d), there is no way to collapse all the WT pdfs on a single curve with a unique exponent H as expected from the self-similarity relationship (14). Instead, this can be done (Arneodo et al., 1997b, 1998c, 1999b) by using a Gaussian kernel that strongly supports the log-normal cascade phenomenology (Castaing et al., 1990; Delour et al., 2001; Kolmogorov, 1962; Oboukhov, 1962) of fully developed turbulence.

3 Generalizing the WTMM Method to d-Dimensional Image Analysis

The generalization of the WTMM method in higher dimension is directly inspired from Mallat *et al.* (Mallat & Hwang, 1992; Mallat & Zhong, 1992) reformulation of Canny multiscale edge detector (Canny, 1986) in terms of 2D WT. The general idea is to start smoothing the discrete image data by convolving it with a filter and then compute the gradient of the smoothed image. This method has been implemented, tested and applied to 2D (Arneodo et al., 1999a, 2000, 2003; Decoster et al., 2000; Roux et al., 2000) and 3D (Kestener & Arneodo, 2003) scalar field.

3.1 The d-Dimensional WTMM Method

Let us define d analyzing wavelet $\psi_i(\mathbf{x} = (x_1, x_2, \ldots, x_d))$ that are respectively, the partial derivatives of a smoothing scalar function $\phi(\mathbf{x})$:

$$\psi_i(\mathbf{x} = (x_1, x_2, \ldots, x_d)) = \partial\phi(\mathbf{x} = (x_1, x_2, \ldots, x_d))/\partial x_i \; , \quad i = 1, 2, \ldots, d. \tag{17}$$

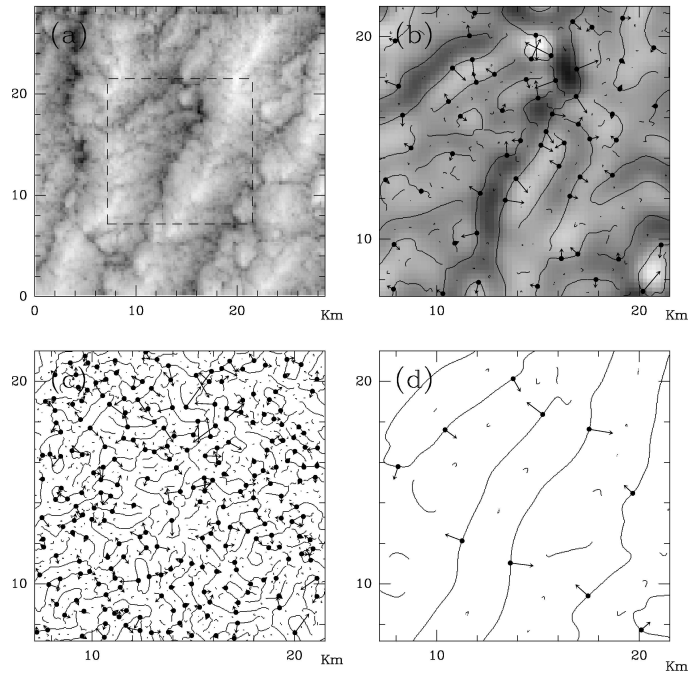

Figure 5 2D wavelet transform analysis of a Landsat image of marine Sc clouds captured at $l = 30$m resolution on July 7,1987, off the coast of San Diego (CA) (Arneodo et al., 1999a; Roux et al., 2000). (a) 256 grey-scale coding of a (1024×1024) portion of the original radiance image. In (b) $a = 2^{2.9}\sigma_W$, (c) $a = 2^{1.9}\sigma_W$ and (d) $a = 2^{3.9}\sigma_W$ (where $\sigma_W = 13$ pixels $\simeq 390$ m), are shown the maxima chains; the local maxima of $\mathcal{M}_{\psi}$ along these chains are indicated by (•) from which originates an arrow whose length is proportional to $\mathcal{M}_{\psi}$ and its direction (with respect to the x-axis) is given by $\mathcal{A}_{\psi}$; only the central (512×512) part delimited by a dashed square in (a) is taken into account to define the WT skeleton. In (b), the smoothed image $\phi_{\mathbf{b},a} * I$ is shown as a grey-scale coded background from white (min) to black (max). $\psi(\mathbf{x})$ is the first-order radially symmetric analyzing wavelet.

$\phi(\mathbf{x})$ is supposed to be an isotropic function that depends on $|\mathbf{x}|$ only and that is well localized around $|\mathbf{x}| = 0$. Commonly used smoothing functions are the Gaussian function :

$$\phi(\mathbf{x} = (x_1, x_2, \ldots, x_d)) = e^{-|\mathbf{x}|^2/2}, \tag{18}$$

and the isotropic Mexican hat :

$$\phi(\mathbf{x} = (x_1, x_2, \ldots, x_d)) = (d - x^2)e^{-|\mathbf{x}|^2/2}, \tag{19}$$

that correspond to a first-order ($n_{\psi} = 1$) and a third-order ($n_{\psi} = 3$) analyzing wavelet respectively.

For any scalar function $f(x_1, x_2, \ldots, x_d) \in L^2(\mathbb{R}^d)$, the WT at point $\mathbf{b}$ and scale a can be expressed in a vectorial form (Arneodo et al., 2000; Decoster et al., 2000; Kestener & Arneodo, 2003):

$$\mathbf{T}_{\psi}[f](\mathbf{b}, a) = \left\{ \begin{array}{l} T_{\psi_1}[f] = a^{-d} \int d^d\mathbf{x}\, \psi_1\big(a^{-1}(\mathbf{x} - \mathbf{b})\big) f(\mathbf{x}) \\ T_{\psi_2}[f] = a^{-d} \int d^d\mathbf{x}\, \psi_2\big(a^{-1}(\mathbf{x} - \mathbf{b})\big) f(\mathbf{x}) \\ \qquad \vdots \\ T_{\psi_d}[f] = a^{-d} \int d^d\mathbf{x}\, \psi_d\big(a^{-1}(\mathbf{x} - \mathbf{b})\big) f(\mathbf{x}) \end{array} \right\} \tag{20}$$

Then, after a straightforward integration by parts, $\mathbf{T}_{\psi}$ can be expressed as the gradient field vector of $f(\mathbf{x})$ smoothed by dilated versions $\phi(\mathbf{x}/a)$ of the smoothing filter. At a given scale a the WTMM are defined by the positions $\mathbf{b}$ where the modulus $\mathcal{M}_{\psi}[f](\mathbf{b}, a) = |\mathbf{T}_{\psi}[f](\mathbf{b}, a)|$ is locally maximum along the direction of the WT vector. These WTMM lie on connected (d-1)

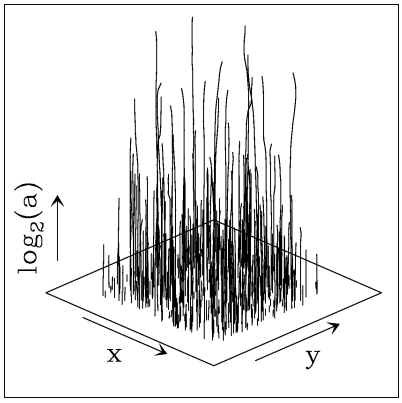

Figure 6 The WT skeleton defined by the maxima lines obtained after linking the WTMMM detected at different scales.

hypersurfaces called maxima hypersurfaces (see Figs 5 and 8). In theory, at each scale a, one only needs to record the position of the local maxima of $\mathcal{M}_{\boldsymbol{\psi}}$ along the maxima hypersurfaces together with the value of $\mathcal{M}_{\boldsymbol{\psi}}[f]$ and the direction $\mathcal{A}_{\boldsymbol{\psi}}[f](\mathbf{b}, a)$ of $\mathbf{T}_{\boldsymbol{\psi}}[f]$. These WTMMM are disposed along connected curves across scales called maxima lines living in a (d+1)-space $(x_1, x_2, \ldots, x_d, a)$. The WT skeleton is then defined as the set of maxima lines that converge to the $(x_1, x_2, \ldots, x_d)$ hyperplane in the limit $a \to 0^+$ (see Fig. 6). As originally demonstrated in Arneodo et al. (1999a), Decoster et al. (2000) and Kestener & Arneodo (2003), the local Hölder regularity of $f(\mathbf{x})$ can be estimated from the power-law behavior of $\mathcal{M}_{\boldsymbol{\psi}}[f]\big(\mathcal{L}_{\mathbf{x}_0}(a)\big) \sim a^{h(\mathbf{x}_0)}$ along the maxima line $\mathcal{L}_{\mathbf{x}_0}(a)$ pointing to the point $\mathbf{x}_0$ in the limit $a \to 0^+$, provided $h(\mathbf{x}_0)$ be smaller than the number $n_{\boldsymbol{\psi}}$ $(= \min_j n_{\psi_j})$ of zero moments of the analyzing wavelet $\boldsymbol{\psi}$. Then, very much like in 1D (Eq. (9)), one can use the scale-partitioning given by the WT skeleton to define the following partition functions :

$$\mathcal{Z}(q, a) = \sum_{\mathcal{L} \in \mathcal{L}(a)} \left(\mathcal{M}_{\boldsymbol{\psi}}[f](\mathbf{x}, a)\right)^q \ , \tag{21}$$

where $q \in \mathbb{R}$ and $\mathcal{L}(a)$ is the set of maxima lines that exist at scale a in the WT skeleton. As before, the $\tau(q)$ spectrum will be extracted from the scaling behavior of $\mathcal{Z}(q, a)$ (Eq. (10)) and in turn the $D(h)$ singularity spectrum will be obtained from the Legendre transform of $\tau(q)$ (Eq. (11)) (Arneodo et al., 1999a; Decoster et al., 2000; Kestener & Arneodo, 2003).

3.2 Application of the 2D WTMM Method to High-Resolution Satellite Images of Cloud Structure

Stratocumulus are one of the most studied clouds types (Davis et al., 1996). Being at once persistent and horizontal extended, marine Sc layers are responsible for a large portion of the earth's global albedo, hence , its overall energy balance. Figure 5(a) shows a typical 1024x1024 pixels portion among 14 overlapping subscenes of the original Sc Landsat images where quasi-nadir viewing radiance at satellite level is digitized on an eight-bit grey scale. The different steps of the 2D WTMM methodology are illustrated in Fig. 5 (b,c,d) where the WTMM chains and the local maxima of $\mathcal{M}_{\boldsymbol{\psi}}$ along these chains computed with the first order ($n_{\boldsymbol{\psi}} = 1$) analyzing wavelet, are shown at different scales. In Fig. 7 are reported the $\tau(q)$ and $D(h)$ multifractal spectra obtained from the scaling behavior of $\mathcal{Z}(q, a)$ over the range of scales 390 m $\lesssim a \lesssim$ 3120 m (Arneodo et al., 1999a; Roux et al., 2000). Both spectra are clearly non linear and very well fitted by the theoretical quadratic spectra of log-normal cascade processes (Eqs (15) and (16) with $d = 2$). However, with the first-order analyzing wavelet, the best fit is obtained with the parameter values $c_1 = 0.38 \pm 0.02$ and $c_2 = 0.070 \pm 0.005$, while for the third-order wavelet these parameters take slightly different values, namely $c_1 = 0.37 \pm 0.02$ and $c_2 = 0.060 \pm 0.005$. The intermittency

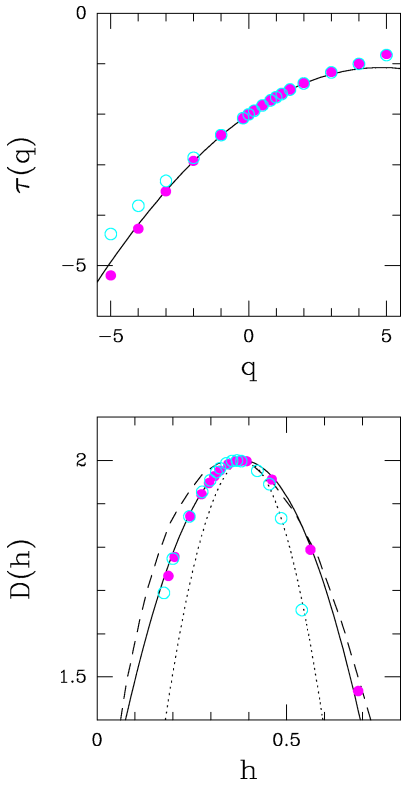

Figure 7 Determination of the multifractal spectra of radiance Landsat images of marine Sc using the 2D WTMM method with either a first order (•) or a third-order (○) radially symmetric analyzing wavelet (Eqs (17,18) and (17,19) respectively). $\tau(q)$ *vs* q; (b) $D(h)$ *vs* h, In (a) and (b), the solid lines correspond to the theoretical multifractal spectra for log-normal cascade processes namely, Eqs (15) and (16) with parameter values $c_1 = 0.38$ and $c_2 = 0.07$ and $d = 2$. The $D(h)$ singularity spectrum of longitudinal velocity (dotted line) and temperature (dashed line) fluctuations in fully developed turbulence are shown for comparison in (b).

coefficient c_2 is therefore somehow reduced when going from $n_\psi = 1$ to $n_\psi = 3$. Actually, it is a lack of statistical convergence because of insufficient sampling which is the main reason for this uncertainty in the estimate of c_2.

In Fig.7(b) are shown for comparison the $D(h)$ singularity spectra of turbulent longitudinal velocity data recorded at the Modane wind tunnel ($R_\lambda \simeq 2000$) and of temperature fluctuations recorded in a $R_\lambda = 400$ turbulent flow (Ruiz-Chavarria et al., 1996). The $D(h)$ curve for marine Sc clouds is much wider than the velocity $D(h)$ spectrum (the intermittency coefficient c_2 being almost three time larger) and it is rather close to the temperature $D(h)$ spectrum. If it is well recognized that liquid water is not really passive, the results derived with the 2D WTMM method in Fig. 7 show that from a multifractal point of view, the intermittency captured by the Landsat satellite looks statistically equivalent to the intermittency of a passive scalar in fully developed 3D turbulence. The fact that the internal structure of Sc cloud somehow reflects some statistical properties of atmospheric turbulence is not such a surprise in this highly turbulent environment (Arneodo et al., 1999a; Roux et al., 2000).

3.3 Application of the 3D WTMM Method to 3D Isotropic Turbulence Simulations

A central quantity in the K41 theory of fully developed turbulence is the mean energy dissipation $\epsilon = \frac{\nu}{2} \sum_{i,j} (\partial_j v_i + \partial_i v_j)^2$ which is supposed to be constant. Indeed, ϵ is not spatially homogeneous

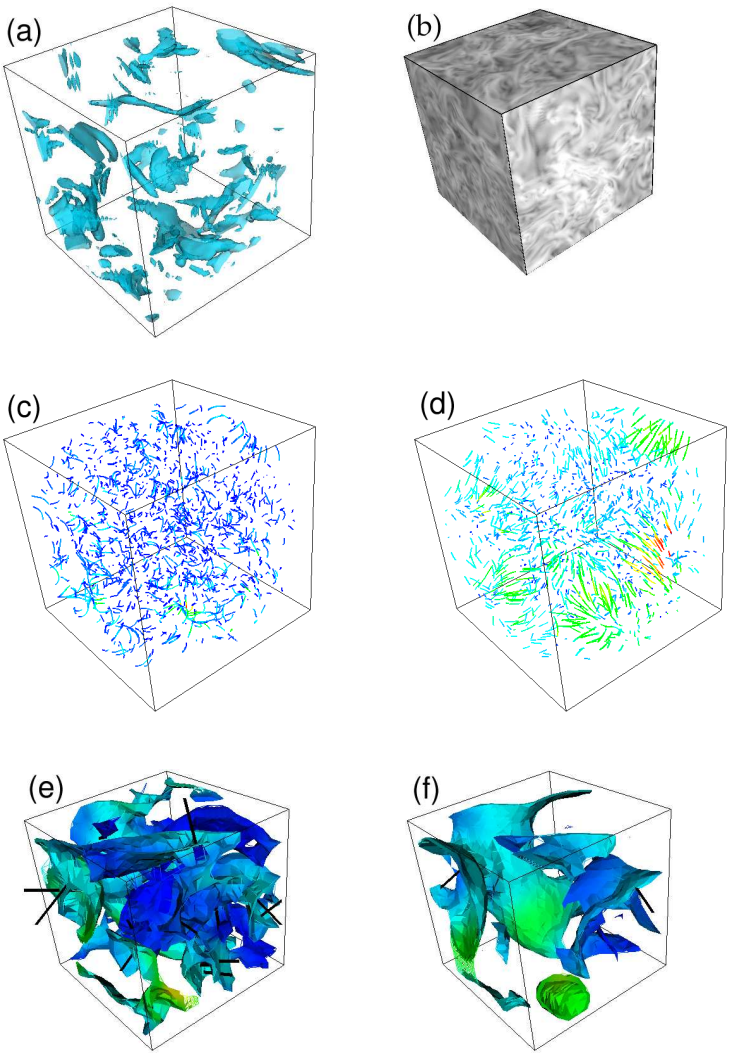

Figure 8 3D WT analysis of the DNS dissipation field ϵ. ψ is the first-order analyzing wavelet ($\phi(\mathbf{x})$ is the Gaussian). (a) Isosurface plot of ϵ in a $(128)^3$ subcube. (b) $\log(\epsilon)$ in the $(128)^3$ central part as coded using 64 grey levels. (c) Field lines of $\mathbf{T}_\psi[f](\mathbf{b}, a)$ for $a = \sigma_W = 7$ pixels. (d) Same as (c) for $a = 2\sigma_W$. (e) WTMM surfaces at scale $a = 2\sigma_W$; from the WTMMM along these surfaces originates a black segment whose length is proportional to $\mathcal{M}_\psi$ and direction is along the WT vector; the colors on the WTMM surfaces are proportional to $\mathcal{M}_\psi$. (f) same as (e) for $a = 4\sigma_W$.

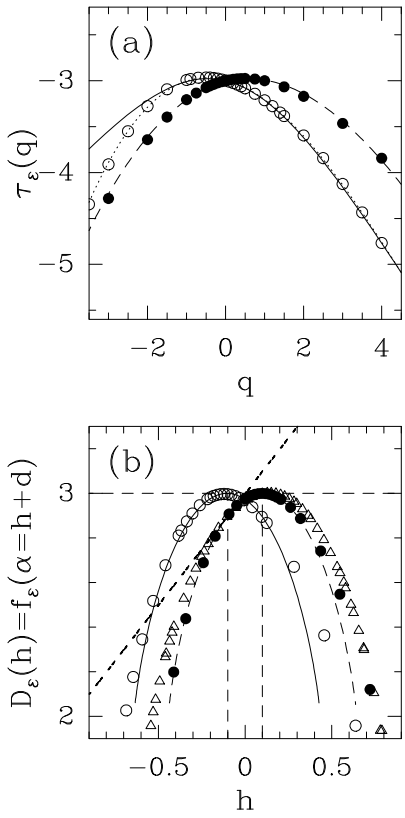

Figure 9 Multifractal analysis of Meneguzzi DNS simulation data ($d = 3$). using the 3D WTMM method (○) and BC techniques (●). (a) $\tau_\epsilon(q) = \tau_\epsilon^{\rm WT}(q)$ or $\tau_\epsilon^{\rm BC}(q) - 3q$ *vs* q; the solid (dashed) lines correspond to the p-model with weights $p_1 = 0.36$, $p_2 = 0.78$ ($p_1 = 0.32$, $p_2 = 0.68$). (b) $D_\epsilon(h) = D_\epsilon^{\rm WT}(h)$ or $D_\epsilon^{\rm BC}(h) = f_\epsilon^{\rm WT}(h+3)$; the solid and dashed lines have the same meaning as in (a); the (△) correspond to some average $D_{\epsilon'}^{\rm BC}(h)$ spectrum of experimental ($d = 1$) surrogate dissipation data (Meneveau & Sreenivasan, 1991).

but undergoes local intermittent fluctuations (Frisch, 1995; Meneveau & Sreenivasan, 1991). There have been early numerical and experimental attempts to measure the multifractal spectra of ϵ or of its 1D surrogate approximation $\epsilon' = 15\nu(\partial u/\partial x)^2$ (where u is the longitudinal velocity) using classical box counting techniques (Meneveau & Sreenivasan, 1991). In Figs. 8 and 9 are reported the results of the application of the 3D WTMM method (Kestener & Arneodo, 2003) to isotropic turbulence direct numerical simulations (DNS) data obtained by Meneguzzi with the same numerical code as previously used by Vincent & Meneguzzi (1991), but at a $(512)^3$ resolution and a viscosity of 5.10^{-4} corresponding to a Taylor Reynolds number $R_\lambda = 216$ (one snapshot of the dissipation 3D spatial field). The main steps of the 3D WT computation are illustrated in Fig. 8. Note that the WTMMM points that define the WT skeleton, now lie on WTMM 2D surfaces at a given scale. The multifractal spectra obtained from this WT skeleton are shown in Fig. 9. The $\tau_\epsilon(q)$ spectrum in Fig. 9(a) significantly deviates from a straight line the hallmark of multifractality. But surprisingly, the data obtained from the 3D WTMM method $\tau_\epsilon^{\rm WT}(q)$ significantly differ from the spectrum $\tau_\epsilon(q) = \tau_\epsilon^{\rm BC}(q) - 3q$ estimated with box-counting technique (Kestener & Arneodo, 2003). Actually the WT estimate of the cancellation exponent $\tau_\epsilon^{\rm WT}(q=1) + 3 = -0.19 \pm 0.03 < 0$, the signature of a signed measure. Indeed, as shown in Fig. 9(a), the $\tau_\epsilon^{\rm WT}(q)$ data are rather nicely fitted by the theoretical spectrum $\tau_\mu(q)$ of the nonconservative binomial p model (Mandelbrot, 1974; Meneveau & Sreenivasan, 1991) with weights $p_1 = 0.36$ and $p_2 = 0.78$ ($p_1 + p_2 = 1.14 > 1$). By construction, the BC algorithms systematically

provide a misleading conservative $\tau_\epsilon(q)$ spectrum diagnostic with $p = p_1/(p_1 + p_2) = 0.32$ and $1 - p = p_2/(p_1 + p_2) = 0.68$. The difference between the two spectra is nothing but a fractional integration of exponent $H^* = \log_2(p_1 + p_2) \sim 0.19$. This result is confirmed in Fig. 9(b) where the singularity spectrum $D_\epsilon^{\rm BC}(h)$ is misleadingly shifted to the right by H^* (= − the cancellation exponent), without any change of shape as compared to $D_\epsilon^{\rm WT}(h)$ (Kestener & Arneodo, 2003). This observation seriously questions the validity of most of the experimental and numerical BC estimates of $\tau_\epsilon^{\rm BC}(q)$ and $f_\epsilon^{\rm BC}(\alpha) = D_\epsilon^{\rm BC}(h + 3)$ spectra reported so far in the literature. Besides the fact that the $\tau_\epsilon^{\rm WT}(q)$ and $D_\epsilon^{\rm WT}(h)$ spectra seem to be even better fitted by a parabola, as predicted for non-conservative log-normal cascade processes, these results raise the fundamental question of the possible asymptotic decrease to zero of the cancellation exponent in the infinite Reynolds number limit.

4 Perspectives

For many years, the multifractal description has been mainly devoted to scalar measures and functions. However, in physics as well as in other fundamental and applied sciences, fractals appear not only as deterministic or random scalar fields but also as vector-valued deterministic or random fields. Very recently, Kestener & Arneodo (2004, 2007) have combined singular value decomposition techniques and WT analysis to generalize the multifractal formalism to vector-valued random fields. The so-called Tensorial Wavelet Transform Modulus Maxima (TWTMM) method has been applied to turbulent velocity and vorticity fields generated in $(256)^3$ DNS of the incompressible Navier-Stokes equations. This study reveals the existence of an intimate relationship $D_V(h + 1) = D_\omega(h)$ between the singularity spectra of these two vector fields that are found significantly more intermittent that previously estimated from longitudinal and transverse velocity increment statistics. Furthermore, thanks to the singular value decomposition, the TWTMM method looks very promising for future simultaneous multifractal and structural (vorticity sheets, vorticity filaments) analysis of turbulent flows (Kestener & Arneodo, 2004, 2007).

References

P. Abry, P. Flandrin, M. S. Taqqu & D. Veitch (2000). Wavelets for the analysis, estimation and synthesis of scaling data. In *Self Similar Network Traffic Analysis and Performance Evaluation* (K. Park & W. Willinger, eds.), pp. 39–88. Wiley.

P. Abry, R. Baraniuk, P. Flandrin, R. Riedi & D. Veitch (2002a). Multiscale nature of network traffic. *IEEE Signal Process. Mag.* **19**, 28–46.

P. Abry, P. Flandrin, M. S. Taqqu & D. Veitch (2002b). Self-similarity and long-range dependence through the wavelet lens. In *Theory and Applications of Long Range Dependence* (P. Doukhan, G. Oppenheim & M. S. Taqqu, eds.). Birkhauser, Boston.

F. Anselmet, Y. Gagne, E. J. Hopfinger & R. A. Antonia (1984). High-order velocity structure functions in turbulent shear flows. *J. Fluid Mech.* **140**, 63–89.

F. Argoul, A. Arneodo, J. Elezgaray & G. Grasseau (1990). Wavelet analysis of the self-similarity of diffusion-limited aggregates and electrodeposition clusters. *Phys. Rev. A* **41**, 5537–5560.

A. Arneodo, G. Grasseau & M. Holschneider (1988). Wavelet transform of multifractals. *Phys. Rev. Lett.* **61**, 2281–2284.

A. Arneodo, F. Argoul, J. Elezgaray & G. Grasseau (1989). Wavelet transform analysis of fractals: application to nonequilibrium phase transitions. In *Nonlinear Dynamics* (G. Turchetti, ed.), pp. 130–180. World Scientific, Singapore.

A. Arneodo, F. Argoul, E. Bacry, J. Elezgaray, E. Freysz, G. Grasseau, J.-F. Muzy & B. Pouligny (1992). Wavelet transform of fractals. In *Wavelets and Applications* (Y. Meyer, ed.), pp. 286 – 352. Springer, Berlin.

A. Arneodo, E. Bacry, P. V. Graves & J.-F. Muzy (1995a). Characterizing long-range correlations in DNA sequences from wavelet analysis. *Phys. Rev. Lett.* **74**, 3293–3296.

A. Arneodo, E. Bacry & J.-F. Muzy (1995b). The thermodynamics of fractals revisited with wavelets. *Physica A* **213**, 232–275.

A. Arneodo, Y. d'Aubenton-Carafa, E. Bacry, P. V. Graves, J.-F. Muzy & C. Thermes (1996). Wavelet based fractal analysis of DNA sequences. *Physica D* **96**, 291–320.

A. Arneodo, E. Bacry, S. Jaffard & J.-F. Muzy (1997a). Oscillating singularities on Cantor sets: A grand-canonical multifractal formalism. *J. Stat. Phys.* **87**, 179–209.

A. Arneodo, J. F. Muzy & S. G. Roux (1997b). Experimental analysis of self-similarity and random cascade processes: Application to fully developed turbulence data. *J. Physique II* **7**, 363–370.

A. Arneodo, B. Audit, E. Bacry, S. Manneville, J.-F. Muzy & S. G. Roux (1998a). Thermodynamics of fractal signals based on wavelet analysis: application to fully developed turbulence data and DNA sequences. *Physica A* **254**, 24–45.

A. Arneodo, E. Bacry, S. Jaffard & J.-F. Muzy (1998b). Singularity spectrum of multifractal functions involving oscillating singularities. *J. of Fourier Anal. & Appl.* **4**, 159–174.

A. Arneodo, S. Manneville & J.-F. Muzy (1998c). Towards log-normal statistics in high reynolds number turbulence. *Eur. Phys. J. B* **1**, 129–140.

A. Arneodo, N. Decoster & S. G. Roux (1999a). Intermittency, log-normal statistics, and multifractal cascade process in high-resolution satellite images of cloud structure. *Phys. Rev. Lett.* **83**, 1255–1258.

A. Arneodo, S. Manneville, J.-F. Muzy & S. G. Roux (1999b). Revealing a lognormal cascading process in turbulent velocity statistics with wavelet analysis. *Phil. Trans. R. Soc. Lond. A* **357**, 2415–2438.

A. Arneodo, N. Decoster & S. G. Roux (2000). A wavelet-based method for multifractal image analysis. I. Methodology and test applications on isotropic and anisotropic random rough surfaces. *Eur. Phys. J. B* **15**, 567–600.

A. Arneodo, B. Audit, N. Decoster, J.-F. Muzy & C. Vaillant (2002). Wavelet based multifractal formalism: Application to DNA sequences, satellite images of the cloud structure and stock market data. In *The Science of Disasters: Climate Disruptions, Heart Attacks, and Market Crashes* (A. Bunde, J. Kropp & H. J. Schellnhuber, eds.), pp. 26–102. Springer Verlag, Berlin.

A. Arneodo, N. Decoster, P. Kestener & S. G. Roux (2003). A wavelet-based method for multifractal image analysis: From theoretical concepts to experimental applications. *Adv. Imaging Electr. Phys.* **126**, 1–92.

B. Audit, C. Thermes, C. Vaillant, Y. d'Aubenton Carafa, J.-F. Muzy & A. Arneodo (2001). Long-range correlations in genomic DNA: a signature of the nucleosomal structure. *Phys. Rev. Lett.* **86**, 2471–2474.

B. Audit, C. Vaillant, A. Arneodo, Y. d'Aubenton Carafa & C. Thermes (2002). Long-range correlations between DNA bending sites: relation to the structure and dynamics of nucleosomes. *J. Mol. Biol.* **316**, 903–918.

E. Aurell, U. Frisch, J. Lutsko & M. Vergassola (1992). On the multifractal properties of the energy-dissipation derived from turbulence data. *J. Fluid Mech.* **238**, 467–486.

E. Bacry, J.-F. Muzy & A. Arneodo (1993). Singularity spectrum of fractal signals from wavelet analysis: exact results. *J. Stat. Phys.* **70**, 635–674.

T. Bohr & T. Tèl (1988). The thermodynamics of fractals. In *Direction in Chaos, Vol. 2* (B. L. Hao, ed.), pp. 194–237. World Scientific, Singapore.

J. Canny (1986). A computational approach to edge-detection. *IEEE Trans. Patt. Anal. Mach. Intell.* **8**, 679–698.

B. Castaing, Y. Gagne & E. J. Hopfinger (1990). Velocity probability density-functions of high Reynolds-number turbulence. *Physica D* **46**, 177–200.

P. Collet, J. Lebowitz & A. Porzio (1987). The dimension spectrum of some dynamical systems. *J. Stat. Phys.* **47**, 609–644.

A. Davis, A. Marshak, W. J. Wiscombe & R. F. Cahalan (1996). Multifractal characterizations of intermittency in nonstationary geophysical signals and fields - A model-based perspective on ergodicity issues illustrated with cloud data. In *Current Topics in Nonstationary Analysis* (G. Treviño, ed.), pp. 97–158. World Scientific, Singapore.

N. Decoster, S. G. Roux & A. Arneodo (2000). A wavelet-based method for multifractal image analysis. II. Applications to synthetic multifractal rough surfaces. *Eur. Phys. J. B* **15**, 739–764.

J. Delour, J.-F. Muzy & A. Arneodo (2001). Intermittency of 1D velocity spatial profiles in turbulence: a magnitude cumulant analysis. *Eur. Phys. J. B* **23**, 243–248.

J. D. Farmer, E. Ott & J. A. Yorke (1983). The dimension of chaotic attractors. *Physica D* **7**, 153–180.

U. Frisch (1995). *Turbulence.* Cambridge University Press, Cambridge.

P. Goupillaud, A. Grossmann & J. Morlet (1984). Cycle-octave and related transforms in seismic signal analysis. *Geoexploration* **23**, 85–102.

P. Grassberger & I. Procaccia (1983). Measuring the strangeness of strange attractors. *Physica D* **9**, 189–208.

P. Grassberger, R. Badii & A. Politi (1988). Scaling laws for invariant measures on hyperbolic and non hyperbolic attractors. *J. Stat. Phys.* **51**, 135 –178.

A. Grossmann & J. Morlet (1984). Decomposition of Hardy functions into square integrable wavelets of constant shape. *S.I.A.M. J. of Math. Anal.* **15**, 723–736.

T. C. Halsey, M. H. Jensen, L. P. Kadanoff, I. Procaccia & B. I. Shraiman (1986). Fractal measures and their singularities: The characterization of strange sets. *Phys. Rev. A* **33**, 1141–1151.

H. G. E. Hentschel (1994). Stochastic multifractality and universal scaling distributions. *Phys. Rev. E* **50**, 243–261.

M. Holschneider (1988). On the wavelet transform of fractal objects. *J. Stat. Phys.* **50**, 963–993.

M. Holschneider & P. Tchamitchian (1990). Régularité locale de la fonction non-différentiable de Riemann. In *Les Ondelettes en 1989* (P. G. Lemarié, ed.), pp. 102–124. Springer, Berlin.

S. Jaffard (1989). Hölder exponents at given points and wavelet coefficients. *C. R. Acad. Sci. Paris Sér. I* **308**, 79–81.

S. Jaffard (1991). Pointwise smoothness, two-microlocalization and wavelet coefficients. *Publ. Mat.* **35**, 155–168.

S. Jaffard (1997a). Multifractal formalism for functions part I: results valid for all functions. *SIAM J. Math. Anal.* **28**, 944–970.

S. Jaffard (1997b). Multifractal formalism for functions part II: self-similar functions. *SIAM J. Math. Anal.* **28**, 971–998.

S. Jaffard, B. Lashermes & P. Abry (2006). Wavelet leaders in multifractal analysis. In *Wavelet Analysis and Applications* (T. Qian, M. I. Vai & Y. Xu, eds.), pp. 219–264. Birkhäuser Verlag, Basel, Switzerland.

P. Kestener & A. Arneodo (2003). Three-dimensional wavelet-based multifractal method: The need for revisiting the multifractal description of turbulence dissipation data. *Phys. Rev. Lett.* **91**, 194501.

P. Kestener & A. Arneodo (2004). Generalizing the wavelet-based multifractal formalism to random vector fields: Application to three-dimensional turbulence velocity and vorticity data. *Phys. Rev. Lett.* **93**, 044501.

P. Kestener & A. Arneodo (2007). A multifractal formalism for vector-valued random fields based on wavelet analysis: application to turbulent velocity and vorticity 3D numerical data. *Stoch. Environ. Res. Risk Assess. DOI: 10.1007/s00477-007-0121-6* .

P. Kestener, J.-M. Lina, P. Saint-Jean & A. Arneodo (2001). Wavelet-based multifractal formalism to assist in diagnosis in digitized mammograms. *Image Anal. Stereol.* **20**, 169–174.

A. N. Kolmogorov (1941). The local structure of turbulence in incompressible viscous fluid for very large Reynolds numbers. *C. R. Acad. Sci. URSS* **30**, 301–305.

A. N. Kolmogorov (1962). A refinement of previous hypotheses concerning the local structure of turbulence in a viscous incompressible fluid at high Reynolds number. *J. Fluid Mech.* **13**, 82–85.

S. Mallat & W. Hwang (1992). Singularity detection and processing with wavelets. *IEEE Trans. Info. Theory* **38**, 617–643.

S. Mallat & S. Zhong (1992). Characterization of signals from multiscale edges. *IEEE Trans. Patt. Recog. Mach. Intell.* **14**, 710–732.

B. B. Mandelbrot (1974). Intermitttent turbulence in self-similar cascades: divergence of high moments and dimension of the carrier. *J. Fluid Mech.* **62**, 331–358.

C. Meneveau & K. R. Sreenivasan (1991). The multifractal nature of turbulent energy-dissipation. *J. Fluid Mech.* **224**, 429–484.

A. S. Monin & A. M. Yaglom (1975). *Statistical Fluid Mechanics: Mechanics of turbulence*, vol. 2. MIT Press, Cambridge, MA.

J.-F. Muzy, E. Bacry & A. Arneodo (1991). Wavelets and multifractal formalism for singular signals: Application to turbulence data. *Phys. Rev. Lett.* **67**, 3515–3518.

J.-F. Muzy, E. Bacry & A. Arneodo (1993). Multifractal formalism for fractal signals: The structure-function approach versus the wavelet-transform modulus-maxima method. *Phys. Rev. E* **47**, 875–884.

J.-F. Muzy, E. Bacry & A. Arneodo (1994). The multifractal formalism revisited with wavelets. *Int. J. Bifurc. Chaos* **4**, 245–302.

A. M. Oboukhov (1962). Some specific features of atmospheric tubulence. *J. Fluid Mech.* **13**, 77–81.

G. Paladin & A. Vulpiani (1987). Anomalous scaling laws in multifractal objects. *Phys. Rep.* **156**, 147–225.

G. Parisi & U. Frisch (1985). Fully developed turbulence and intermittency. In *Turbulence and Predictability in Geophysical Fluid Dynamics and Climate Dynamics* (M. Ghil, R. Benzi & G. Parisi, eds.), Proc. of Int. School, pp. 84–88. North-Holland, Amsterdam.

C.-K. Peng, S. V. Buldyrev, A. L. Goldberger, S. Havlin, F. Sciortino, M. Simons & H. E. Stanley (1992). Long-range correlations in nucleotide sequences. *Nature* **356**, 168–170.

D. Rand (1989). The singularity spectrum for hyperbolic Cantor sets and attractors. *Ergod. Th. Dyn. Sys.* **9**, 527–541.

S. G. Roux, A. Arneodo & N. Decoster (2000). A wavelet-based method for multifractal image analysis. III. Applications to high-resolution satellite images of cloud structure. *Eur. Phys. J. B* **15**, 765–786.

G. Ruiz-Chavarria, C. Baudet & S. Ciliberto (1996). Scaling laws and dissipation scale of a passive scalar in fully developed turbulence. *Physica D* **99**, 369–380.

D. Veitch & P. Abry (1999). A wavelet-based joint estimator of the parameters of long-range dependence. *IEEE Trans. Info. Theo.* **45**, 878–897.

A. Vincent & M. Meneguzzi (1991). The spatial structure and statistical properties of homogeneous turbulence. *J. Fluid Mech.* **225**, 1–20.

R. F. Voss (1992). Evolution of long-range fractal correlations and $1/f$ noise in DNA base sequences. *Phys. Rev. Lett.* **68**, 3805–3808.

H. Wendt & P. Abry (2007). Multifractality tests using bootstrapped wavelet leaders. *IEEE Trans. Signal Process.* **55**, 4811–4820.

H. Wendt, P. Abry & S. Jaffard (2007). Bootstrap for empirical multifractal analysis. *IEEE Signal Process. Mag.* **24**, 38–48.